A Multiresolution Approach to Target Detection in Synthetic Aperture Radar Data

Nikola S. Subotic, Leslie M. Collins, John D. Gorman, and Brian J. Thelen
Environmental Research Institute of Michigan
P.O. Box 134001
Ann Arbor, MI 48113-4001
Telephone:(313)-994-1200
email: subotic@erim.org

Abstract

We demonstrate the utility of a multiresolution approach for target detection in SAR imagery. In particular, man-made objects exhibit characteristic phase and amplitude fluctuations as the image resolution is varied, while natural terrain (i.e., clutter) has a random signature. We show that the multiresolution clutter process decomposes into a Brownian motion process in resolution. We then construct an optimal invariant multiresolution detector based on a derived multiresolution increments process and show that it significantly outperforms a standard energy detector operating on the finest available SAR resolution.

Introduction

Many synthetic aperture radar (SAR) target detection algorithms work on a single resolution image at the finest available resolution [6], [7]. However, there is compelling evidence to suggest that significant performance gains can be achieved by casting the detection problem in a multiresolution setting. We argue, using simple physical principles, that this performance gain is a direct result of the coherent interference effects that occur in typical radar target signatures as the imaging resolution is varied.

SAR images of man-made objects typically consist of spatial patterns of bright points and lines resulting from radar backscatter from discrete physical features such as corners, edges, flat plates and other primative geometric shapes. The coherent radar return from each of these discrete features, or *prominent scatterers*, is a complex phasor with amplitude equal to the local radar cross-section of the target feature. At fine enough resolutions, these prominent scatterers are isolated in individual resolution cells and they dominate the target signature. As the resolution changes from fine to coarse, adjacent scatterers become lumped together into a single resolution cell and coherently interfere with each other, leading to characteristic changes in amplitude and phase as a function of resolution. It is this relationship between phase and amplitude as a function of resolution that we exploit through the use of a multiresolution-based detector.

Figure 1 shows three colinear scatterers each of equal amplitude and separated by a distance D. Also shown are the amplitude and phase of a pixel located at the origin, plotted as a function of resolution. One can see that coherent interference effects cause the pixel amplitude and phase to oscillate as the resolution is varied fine to coarse. Beyond a coarse enough resolution, however, all three scatterers are contained in a single resolution cell and the phase and amplitude remain constant.

Natural terrain typically consists of a large collection of small amplitude scatterers that are randomly distributed within each resolution cell. Thus SAR imagery of terrain, i.e., *clutter*, is frequently modeled as a Gaussian random field by appealing to the law of large numbers [10] and references therein. The result is that the amplitude and phase of a clutter pixel vary randomly as a function of resolution. We show that the clutter signature becomes a Brownian motion process as a function of resolution.

Multiresolution Process Statistics

In our construction, we model the scene $c(\underline{x})$, $\underline{x} \in \mathbb{R}^2$ as a collection of point scatterers, in which each point scatterer is specified by its location $\underline{x}_k \in \mathbb{R}^2$ and

1058-6393/95 $4.00 © 1995 IEEE

complex reflectivity $u_k \in \mathbb{C}$:

$$c(\underline{x}) = \sum_{k=1}^{K} u_k \delta(\underline{x} - \underline{x}_k). \quad (1)$$

This approach has been used to model both clutter [10, and references therein] and objects that consist of collections of point reflectors [5, for instance] (i.e., trihedrals or corner reflectors). We refer to c as the complex reflectivity function.

The complex-valued SAR image, taking into account resolution, can be written as a convolution between the complex reflectivity function, $c(\underline{x})$, and the system impulse response, $h(\underline{x})$, [12]:

$$\begin{aligned} T(\underline{x};\rho) &= \frac{1}{\rho}\int c(\underline{y}) h\left(\frac{\underline{x}-\underline{y}}{\rho}\right) d\underline{y} \\ &= \frac{1}{\rho}\sum_{k=1}^{K} u_k h\left(\frac{\underline{x}-\underline{x}_k}{\rho}\right). \end{aligned} \quad (2)$$

If we model the locations $\{\underline{x}_k\}$ as a Poisson point process with intensity $\lambda(\underline{x})$, then $c(\underline{x})$ is a compound point process or marked Poisson process with marks $\{u_k\}$ [11, Chapter 3]. At each resolution, ρ, $T(\underline{x};\rho)$ then forms a filtered Poisson process [11, Chapter 4].

In the next two sections, we consider models for the statistics of the observed radar image, T, under simple assumptions on the statistics of the scatterer locations $\{\underline{x}_k\}$ and their complex reflectivities $\{u_k\}$.

Case 1: Natural Clutter

For natural terrain, i.e., *clutter*, a typical assumption is that each resolution cell in the SAR image a contains a large number of small amplitude scatterers. In this case, we will assume that the marks $\{u_k\}$ are independent, identically distributed (*iid*) random variables with mean zero and covariance $\sigma_c^2 I$ where I is the identity matrix.

Using a slight generalization of a result in [10], we can invoke the Generalized Multivariate Central Limit Theorem [1] to show that the joint density of $T(\underline{x};\rho)$ converges to multivariate Gaussian as the number of scatterers K tends to infinity. in both space and resolution. The mean and covariance of the process are

$$E\{T(\underline{x};\rho)\} = 0, \quad (3)$$

and

$$\begin{aligned} \Sigma(\underline{x},\underline{x}';\rho,\rho') &= R(\underline{x},\underline{x}';\rho,\rho') \\ &= E\{T(\underline{x};\rho)T^*(\underline{x}';\rho')\} \\ &= \frac{\sigma_c^2}{\rho\rho'}\int h\left(\frac{\underline{x}-\underline{y}'}{\rho}\right) h^*\left(\frac{\underline{x}'-\underline{y}'}{\rho'}\right) dy', \end{aligned} \quad (4)$$

where $R(\underline{x},\underline{x}';\rho,\rho')$ is the correlation function of $T(\underline{x},\rho)$, and σ_c is the variance of the iid marks $\{u_k\}$. Note that the covariance function Σ is completely specified by the variance σ_c and the impulse response $h(\underline{x})$.

The choice of the impulse response h influences the statistics of the SAR image $T(\underline{x},\rho)$. This is especially true when examining $T(\underline{x};\rho)$ as a function of resolution. For a specific spatial location $\underline{x}_0 = \underline{x} = \underline{x}' = \underline{0}$, the covariance in resolution becomes

$$\begin{aligned} \Sigma_{\underline{x}_0}(\rho,\rho') &= \Sigma(\underline{0},\underline{0};\rho,\rho') \\ &= \frac{\sigma_c^2}{\rho\rho'}\int h\left(\frac{-\underline{y}}{\rho}\right) h^*\left(\frac{-\underline{y}}{\rho'}\right) d\underline{y}. \end{aligned} \quad (5)$$

If the impulse response is chosen so that the correlation function R satisfies a scaling law condition [13] with respect to resolution, then the process $T(\underline{x};\rho)$ is Gauss-Markov in resolution. For $\rho_l \le \rho \le \rho_u$ the scaling law is

$$R_{\underline{x}_0}(\rho_l,\rho_u) = \frac{R_{\underline{x}_0}(\rho_l,\rho) R_{\underline{x}_0}(\rho,\rho_u)}{R_{\underline{x}_0}(\rho,\rho)}. \quad (6)$$

The scaling law as it pertains to the SAR impulse response becomes

$$\begin{aligned} \int h\left(\frac{-\underline{y}}{\rho_l}\right) h^*\left(\frac{-\underline{y}}{\rho_u}\right) d\underline{y} &= \tfrac{1}{\|h\|^2}\int h\left(\tfrac{-\underline{y}}{\rho_l}\right) h^*\left(\tfrac{-\underline{y}}{\rho}\right) d\underline{y} \\ &\quad \cdot \int h\left(\tfrac{-\underline{y}'}{\rho}\right) h^*\left(\tfrac{-\underline{y}'}{\rho_u}\right) d\underline{y}'. \end{aligned} \quad (7)$$

For the special case where either the impulse response $h(\underline{x})$ is a sinc$(\underline{x})$ or a rect$(\underline{x})$, the scaling relation is satisfied and the process $T(\underline{x};\rho)$ is Gauss-Markov as a function of ρ. The correlation of $T(\underline{x}_0;\rho)$ becomes $R_{\underline{x}_0}(\rho,\rho') = \sigma_c^2/max\{\rho,\rho'\}$ with variance $\sigma^2 = \sigma_c^2/\rho$.

$T(\underline{x};\rho)$ can also be shown to have independent increments in resolution (i.e. for $\rho_1 > \rho_2 > \rho_3$, $E\{[T(\underline{x}_0,\rho_1) - T(\underline{x}_0,\rho_2)][T(\underline{x}_0,\rho_2) - T(\underline{x}_0,\rho_3)]^*\} = 0$). In this case, the clutter process $T(\underline{x}_0,\rho)$ is a Brownian motion process when viewed as a function of $\frac{1}{\rho}$ [8].

The Brownian motion nature of T in resolution can be exploited to provide a simple linear transformation of the process which whitens the process in resolution. Choose a set of resolutions $\rho_1 < \ldots < \rho_i < \rho_{i+1} < \ldots < \rho_N$ where $\rho_{i+1} = \rho_i + \delta\rho_i$. The increments process in resolution is formed by

$$T'(\underline{x}_0;\rho_i) = T(\underline{x}_0;\rho_i + \delta\rho_i) - T(\underline{x}_0;\rho_i) \quad (8)$$

with $\delta\rho_i > 0$. This process has zero mean and is independent from resolution to resolution.

Furthermore, by judicious choice of resolutions $\{\rho_i\}$, the variance of the difference process T' can be made constant from resolution to resolution. We choose adjacent resolutions to satisfy $\frac{1}{\rho_i} - \frac{1}{\rho_{i+1}} = \gamma$. Under this latter condition, the resolution step size $\delta\rho_i$ can be easily shown to be

$$\delta\rho_i = \frac{\gamma\rho_i^2}{1-\gamma\rho_i}. \tag{9}$$

This resolution sampling strategy is shown in Figure 2 for two choices of γ. The resolution sampling is dense at fine resolutions and becomes sparse at coarse resolutions. Define the vector of resolution increments $\underline{T}'_{\underline{x}_0} = \{T'(\underline{x}_0, \rho_1), \ldots, T'(\underline{x}_0, \rho_{N-1})\}^t$ where t denotes vector transpose. Then $\underline{T}'_{\underline{x}_0}$ is a complex Gaussian random vector with distribution $\underline{T}'_{\underline{x}_0} \sim \mathcal{N}_c(\underline{0}, \gamma\sigma_c^2 I)$.

Case 2: Statistics of Cultural Objects

Many man-made or cultural objects typically consist of a small number of large amplitude point scatterers. In the case of our multiresolution analysis, the physical phenomena we wish to explore is the interaction of a small number of local prominent scatterers and the interference patterns that result. The number of local prominent scatterers we wish to examine are typically less than eight. Larger numbers tend to make the SAR signature exhibit zero mean complex Gaussian statistics [3].

We will reformulate the process to have a random and nonrandom component. The point scatterer model will become

$$c(\underline{x}) = \sum_{k=1}^{K} u_k \delta(\underline{x} - \underline{x}_k) + \sum_{k=1}^{K'} a_k \delta(\underline{x} - \underline{x}_k). \tag{10}$$

The first term in Equation 10 will correspond to the clutter model as outlined in Case 1. The second term will correspond to an unknown set of prominent scatterers. The marks $\{a_k\}$ are deterministic but unknown. The spatial distribution of the prominant scatterers is also assumed to be deterministic. $T(\underline{x}; \rho)$ will be multivariate Gaussian with covariance as in Case 1 (Eq. 5). The mean of the process is

$$E\{T(\underline{x}; \rho)\} = \frac{1}{\rho} \sum_{k=1}^{K'} a_k h\left(\frac{\underline{x} - \underline{x}_k}{\rho}\right). \tag{11}$$

In the same spirit as Case 1, we form a vector of increments in resolution, $\underline{T}'_{\underline{x}_0}$. This process is complex Gaussian with distribution $\underline{T}'_{\underline{x}_0} \sim \mathcal{N}_c(\underline{\mu}, \gamma\sigma_c^2 I)$ where $\underline{\mu} = \{\mu_1, \ldots, \mu_i, \ldots, \mu_{N-1}\}^t$ and

$$\begin{aligned} \mu_i &= E\{T'(\underline{x}_0; \rho_i)\} \\ &= \sum_{k=1}^{K'} a_k \left[\frac{1}{\rho_i + \delta\rho_i} h\left(\frac{\underline{x} - \underline{x}_k}{\rho_i + \delta\rho_i}\right) \right. \\ &\quad \left. - \frac{1}{\rho_i} h\left(\frac{\underline{x} - \underline{x}_k}{\rho_i}\right)\right]. \end{aligned} \tag{12}$$

Detection Strategies

We will base our detection strategies on the increments process $T'(\underline{x}_0; \underline{\rho})$. Our detection strategies will exploit information provided by resolution. This information is, in fact, produced by the local spatial signature as it is incorporated into the resolution process. The above developments motivate detectors which exploit the difference in the mean when either clutter or cultural objects are present. The hypotheses under test will be

$$\begin{aligned} H_0: &\quad T'(\underline{x}_0; \underline{\rho}) \sim \mathcal{N}_c(\underline{\mu}, \Sigma_{\underline{x}_0}), \quad \underline{\mu} = \underline{0} \\ H_1: &\quad T'(\underline{x}_0; \underline{\rho}) \sim \mathcal{N}_c(\underline{\mu}, \Sigma_{\underline{x}_0}), \quad \underline{\mu} \neq \underline{0} \end{aligned}$$

with $\Sigma_{\underline{x}_0} = \gamma\sigma_c^2 I$.

We have chosen the composite test due to the severe variability of SAR signatures when collection geometry and object condition are not known. This is opposed to choosing a specific object signature and designing a matched filter to it. There does not exist a uniformly most power test for the above composite hypothesis. The optimal invariant test with respect to scale and orthogonal transformations is the so-called F test [2] where

$$\psi_1(\underline{x}_0) = |\Sigma_{\underline{x}_0}^{-1/2} \underline{T}'_{\underline{x}_0}|^2 = \sum_{i=1}^{N-1} \frac{|T'(\underline{x}_0; \rho_i)|^2}{(N-1)\gamma\hat{\sigma}_c^2} \overset{H_1}{\gtrless} \beta. \tag{13}$$

where $\hat{\sigma}_c^2$ is the estimate of σ_c^2 from surrounding cells assuming no target is present, i.e.,

$$\hat{\sigma}_c^2 = \frac{\sum_{i=1}^{N-1} \sum_{j=1}^{M} |T'(\underline{x}_j; \rho_i)|^2}{M(N-1)}. \tag{14}$$

where $\underline{x}_1, \ldots, \underline{x}_M$ are locations within clutter. The distribution of the test statistic is $\psi_1(\underline{x}_0) \sim F(2(N-1), 2M(N-1))$ under H_0, and $\psi_1(\underline{x}_0) \sim F(2(N-1), 2M(N-1); \sum_{i=1}^{N-1}(\mu_i^2/\gamma\sigma_c^2))$ under H_1. Here $F(m,n)$ is the central F distribution with m and n degrees of freedom. In addition, $F(m,n;\eta)$ is the noncentral F distribution with the same degrees of freedom and noncentricity parameter η. For the case of

large $M(N-1)$, the estimate of $\hat{\sigma}_c^2$ is almost exact. The distributions become a scaled central chi-square under H_0 and a non-central chi-square under H_1.

An alternative test for the mean can be constructed via the correlation coefficient between increments. For clutter, the increments process is uncorrelated. However, when a cultural object is present, there will be a nonzero correlation coefficent due to the presence of a mean value. We construct an unnormalized autocorrelation test [4]

$$\psi_2(\underline{x}_0) = \frac{1}{\hat{\sigma}_c^2} \sum_{i=1}^{N-1} T'(\underline{x}_0; \rho_i) T'^*(\underline{x}_0; \rho_{i+1}) \overset{H_1}{>} \beta. \quad (15)$$

Our baseline test with which we compare the multiresolution test performance is an F test applied to single resolution SAR image data at the finest resolution. This test is

$$\psi_3(\underline{x}_0) = \frac{|T(\underline{x}_0; \rho_i)|^2}{\hat{\sigma}_c^2} \overset{H_1}{>} \beta \quad (16)$$

This test has been used extensively in initial screening algorithms on SAR data[9]. The distribution of this test is the same as $\psi_1(\underline{x}_0)$ with $m = 2$, $n = 2$, and noncentricity parameter μ_1^2/σ_c^2.

Figure 3 shows the synthetic data set which constitutes the basis for our performance study. This is a set of 17 Synthetic Radar Imaging Model (SRIM) images of a Howitzer, each at a multiple of 20^o aspect angles embedded in zero mean circular Complex Gaussian clutter. The resolution of this simulation is 1 foot. Figure 4 shows the Receiver Operating characteristic of these tests when applied to this data set. Noted in the Figure is the test, finest/coarsest resolutions, and number of resolutions used. The multiresolution F test performed the best in this study. Also note that the multiresolution F test using 2 foot data as its finest resolution as well as or better than the single resolution F test at 1 foot resolution.

Conclusion

In this paper we derived the statistics for multiresolution SAR signatures. For the clutter case we appealed to the Generalized Central Limit Theorem to show that the clutter statistics are complex Gaussian. In addition, we showed that under certain aperture weighting conditions, the clutter process in resolution becomes Brownian motion. The Brownian motion process was exploited to simplify the clutter statistics by forming an increments process and by choosing the resolutions to equalize the clutter variance. A target model was presented where a deterministic but unknown set of point scatterers were added to the marked point process clutter model. Two multiresolution detection strategies are proposed to detect cultural objects whereby the mean value of the objects is not assumed known. An optimal invariant test and a correlation test were explored and found to outperform a simple fine resolution energy detector.

Acknowledgements

This research supported by ARPA/STO contract DAAH01-93-C-R346.

References

[1] T. W. Anderson, *An Introduction to Multivariate Statistical Analysis, 2nd Edition,* Wiley, 1984.

[2] S. F. Arnold, *The theory of Linear Models and Multivariate Analysis,* Wiley, 1981.

[3] P. Beckman, and A. Spizzichino, *The Scattering of Electromagnetic Waves From Rough Surfaces,* Artech House, Norwood, MA (1987).

[4] P. J. Brockwell and R. A Davis, *Time Series: Theory and Methods,* Springer, 1987.

[5] S. R. DeGraaf, "Sidelobe Reduction via FIR filtering in SAR Imagery," *IEEE Trans. Image Proc.*, vol 3, no. 3, 1994.

[6] E. J. Kelly, "An adaptive detection algorithm," *IEEE T Aero. Elec. Sys.*, AES-22, 1, 1986.

[7] G. Minler and J. Minkler, *CFAR: The Principles of Automatic Radar Detection in Clutter,* Magellan, Baltimore, 1990.

[8] Papoulis, A., *Probability, Random Variables and Stochastic Processes,* McGraw-Hill, New York, (1965).

[9] S. R. Sullivan, et. al., "Strategic Target Algorithm Research (STAR) - Final Report," Contract Number F19628-90-C-0002, 1991, SECRET.

[10] B. J. Thelen, "Complete characterization of complex distributions from weak scatterers, *J. Opt. Soc. Amer., ser. A*, in review, 1994.

[11] D. Snyder, *Random Point Processes,* Wiley, 1975.

[12] Walker, J. L., "Range-Doppler Imaging of Rotating Objects," *IEEE Trans. Aerosp. Electron. Syst.*, vol. **AES- 16**, p. 23, Jan. 1980.

[13] Wong, E., and Hajek, B., *Stochastic Processes in Engineering Systems*, Springer, Berlin, (1985).

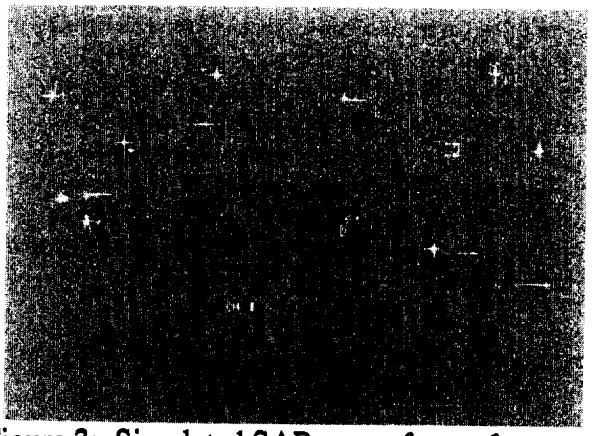

Figure 3: Simulated SAR scene for performance analysis studies

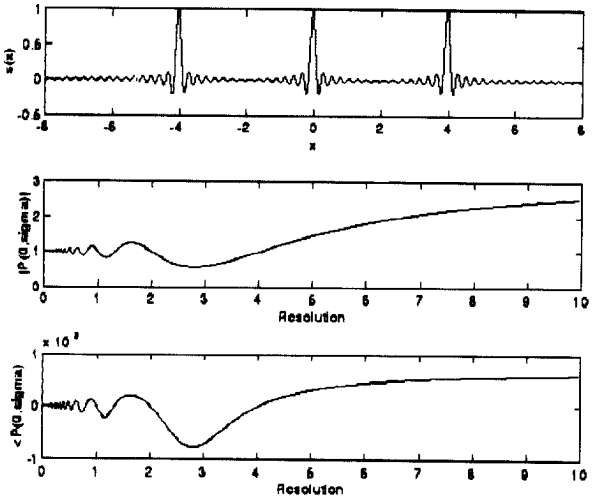

Figure 1. A 1-D Cut Through the Three-Scatter Signal and Multiresolution Amplitude and Phase Fluctuations.

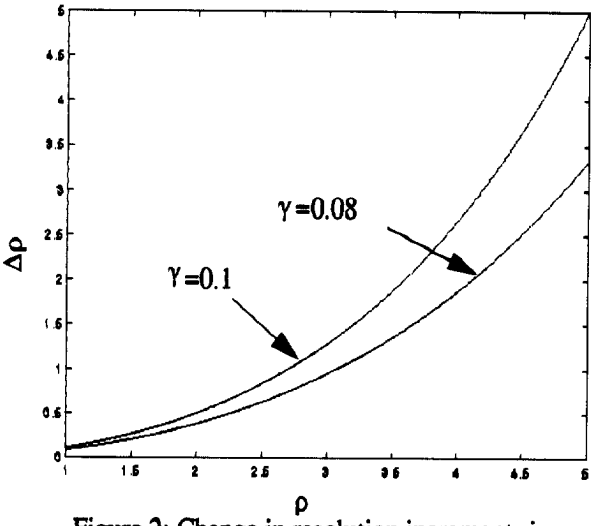

Figure 2: Change in resolution increment size vs. resolution.

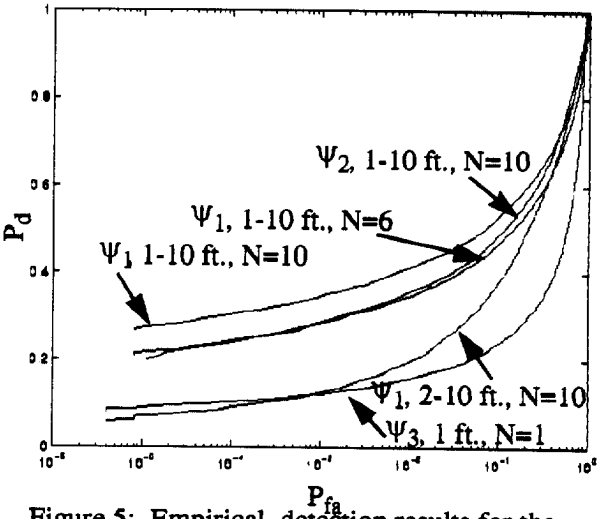

Figure 5: Empirical detection results for the three detection strategies on synthetic data